


Article

Production of Fe–Ti Alloys from Mixed Slag Containing Titanium and Fe_2O_3 via Direct Electrochemical Reduction in Molten Calcium Chloride

Bo Wang ^{1,2} , Chao-yi Chen ^{1,2,*}, Jun-qi Li ^{1,2}, Lin-zhu Wang ^{1,2}, Yuan-pei Lan ^{1,2} and Shi-yu Wang ^{1,2}

¹ College of Materials and Metallurgy, Guizhou University, Guiyang 550025, China; bowang1996@126.com (B.W.); jqli@gzu.edu.cn (J.-q.L.); lzwang@gzu.edu.cn (L.-z.W.); yplan@gzu.edu.cn (Y.-p.L.); sywang17@outlook.com (S.-y.W.)

² Guizhou Province Key Laboratory of Metallurgical Engineering and Process Energy Saving, Guiyang 550025, China

* Correspondence: cychen@gzu.edu.cn; Tel.: +86-150-8601-5817

Received: 8 October 2020; Accepted: 27 November 2020; Published: 30 November 2020



Abstract: High-purity intermetallic β -Ti (FeTi_4) and FeTi alloys were prepared via molten salt electrolysis from a titanium-containing waste slag and Fe_2O_3 mixture using molten CaCl_2 salt as the electrolyte. The mixed slag powders were pressed into a pellet that served as a cathode, while a graphite rod served as an anode. The electrochemical process was conducted at 900 °C with a cell voltage of 3.1 V under an inert atmosphere. The formation process of the alloys and the influence of the Ti:Fe atomic ratio on the product were investigated. With an increased proportion of Ti, the phase of the product changed from FeTi/ Fe_2Ti to FeTi/ FeTi_4 , and different structures were observed. At a Ti:Fe ratio of 1.2:1 in the raw slag, an alloy with a sponge-like morphology and a small amount of FeTi_4 were obtained. During the initial stages of electrolysis, a large amount of intermediate product (CaTiO_3) was formed, accompanied by an abrupt decrease in current and increase in particle size. The current then increased and Fe_2Ti alloy was gradually formed. Finally, as the reaction process extended inside the pellet, the current remained stable and the product mainly contained FeTi and FeTi_4 phases. The observed stages, i.e., $\text{CaTiO}_3(\text{TiO}_2) \rightarrow \text{Fe}_2\text{Ti}(\text{Ti}) \rightarrow \text{FeTi}(\text{FeTi}_4)$, were consistent with the thermodynamic analysis.

Keywords: waste slag containing titanium; molten salt electrolysis; ferro-titanium alloy; FeTi_4

1. Introduction

Ferrotitanium alloys are well-known hydrogen storage materials [1,2] that can be produced by various processes, such as the carbothermic or metallothermic reduction of oxide ores or concentrates. In carbothermic reductions, carbon in the form of coke, coal, or charcoal is used as a reducing agent. In metallothermic reductions, the main reducing agent is aluminum. Iron and titanium metals are common raw materials used for the synthesis of ferrotitanium alloys [3]. Waste slag containing titanium (50.15%) is generally formed during the production of sponge titanium via the Kroll process. On average, more than 200 kg of titanium-containing waste slag is produced per ton of titanium tetrachloride [4]. Owing to the small size of the slag, addition of titanium-containing waste slag at more than 15% will block the furnace, reducing the recovery efficiency. Therefore, the development of an effective method to extract titanium from the titanium-containing slag is crucial and should be investigated.

After nearly 20 years of research, the Fray–Farthing–Chen (FFC) Cambridge process has been successfully applied to the preparation of titanium, tantalum, tungsten, niobium, and other metals and alloys [5–7]. Several studies on the synthesis of Fe–Ti alloy have also been conducted by the FFC process. Zhou et al. [8] successfully prepared Fe–Ti alloys using ilmenite as a precursor at 973 K and 3.2–4.4 V. Tan et al. [9] electrolyzed the mixtures of TiO_2 and Fe_2O_3 to produce ferrotitanium alloys containing intermetallic Fe–Ti phases, such as FeTi and Fe_2Ti , by the FFC process. However, the produced alloys generally contained porous structures with numerous carbon impurities, and no effective method has been proposed to solve this problem. Panigrahi et al. [10] prepared a dense highly purified intermetallic solid of β -Ti (FeTi_4) and FeTi from mixed TiO_2 and FeTiO_3 , at a molar ratio of 5.44:1.00. Owing to the dense structure of the product, the quantity of carbon particle inclusions was relatively low. To date, ferrotitanium alloys have primarily been prepared by electrolysis of FeTiO_3 , or by a mixture of TiO_2 and Fe_2O_3 [11–13]. No research has been reported on the preparation of Ti–Fe alloys from a waste slag containing titanium, because waste slag commonly comprises Si, Ca, and Al. However, it is desirable to use the titanium-bearing slag as a raw material to produce Fe–Ti alloy if the impurities contained in waste slag can be removed by molten salt electrolysis.

The purpose of this study is to produce a Fe–Ti alloy with a dense structure to suppress carbon impurities by the electrochemical reduction of titanium-containing waste slag, which was realized via the FFC method. We aim to explore the influence of the atomic ratio of Ti and Fe in the raw material on the products of electrolysis and investigate the iron alloying process. The results from this study may provide a theoretical basis and general guideline for the industrial production of ferrotitanium alloy from waste titanium-bearing slag.

2. Materials and Methods

2.1. Materials and Characterization Methods

The titanium-bearing waste residue (slag) used in this experiment was obtained from Zunyi Titanium Industry Co., Ltd. The elemental composition of the waste residue is listed in Table 1. The Ti content is 50.15 wt%, and the main impurities are Al, Si, and O. The X-ray diffraction (XRD) pattern of the titanium-containing waste slag (Figure 1) demonstrates that the main phases present are titanium oxides: FeTi_2O_5 , Ti_3O_5 , and TiO_2 . To produce a mixed oxide cathode, the titanium-containing slag and Fe_2O_3 were mixed in a ratio of 1.2:1. The mixture was then ball-milled for 10 h and sintered at 950 °C for 2 h.

Table 1. Elemental composition of titanium-containing slag (wt%).

Elements	Ti	O	Al	Si	Ca	Fe	Mn	Mg
Content (wt%)	50.15	40.65	1.22	2.01	0.65	3.61	1.43	0.28

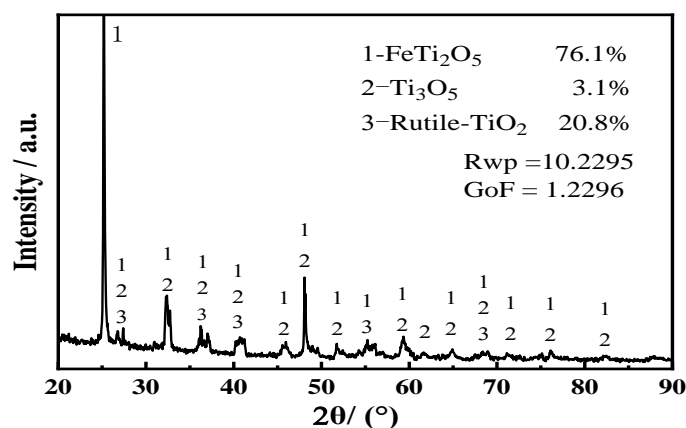


Figure 1. XRD patterns of the titanium slag.

The microstructure and composition of the sintered and electrolyzed pellets were determined by scanning electron microscopy (SEM; EM-30PLUS, Coxem, Korea) coupled with energy-dispersive X-ray spectroscopy (EDS). The pellet phase composition was determined by XRD (X'Pert PRO MPD, PANalytical, The Netherlands). The particle size was determined using the Beckman Coulter LS 13 320 Particle Size Analyzer.

2.2. Experimental Method

The titanium-containing waste residue was mixed with Fe_2O_3 and ball-milled for 10 h, using 8 wt% liquid paraffin as a binder. The mixture was then compressed into pellets with a diameter and height of 10 and 4 mm, respectively, under a pressure of 2 MPa. The pellets were sintered in air at 950 °C for 2 h; the sintered pellet was then wrapped with nickel foam and attached to an iron–chromium–aluminum wire (diameter = 1.5 mm) to form a cathode. The electrolyte was anhydrous CaCl_2 (>96 wt%) contained in a graphite crucible (inner diameter = 50 mm, height = 110 mm).

The graphite crucible containing the molten salt was placed in a vertical cylindrical tube furnace for the electrolysis of the solid pellets. The electrolytic cell was heated to 120 °C under a high-purity Ar atmosphere to remove any physical water. Subsequently, the electrolytic cell was heated up to 550 °C to remove chemically bound water and then to 782 °C to form molten salt electrolyte, and a blank cathode (nickel foam without a pellet) attached with an iron–chromium–aluminum wire was inserted into the molten salt for the pre-electrolysis process. A constant voltage of 2 V was applied between the blank cathode and anode, which were positioned approximately 30 mm apart. The pre-electrolysis process was controlled using an electrochemical workstation (HCP-803, Biologic, Houston, TX, USA) interfaced with a computer, and the current–time curves were recorded.

After the pre-electrolysis process, the voltage was adjusted to 3.1 V (between the oxide cathode and anode), and the electrolysis was terminated after 6 h. After the electrolysis, the cathode was removed from the molten salt and cooled to room temperature (20–25 °C) under an Ar atmosphere. The cathode pellet was washed with distilled water to remove the solidified salt, rinsed with 1 N aqueous hydrochloric acid (HCl) to expel the salt residues in the pores of the pellet, and dried in a vacuum dryer. A schematic illustration of the experimental setup is shown in Figure 2.

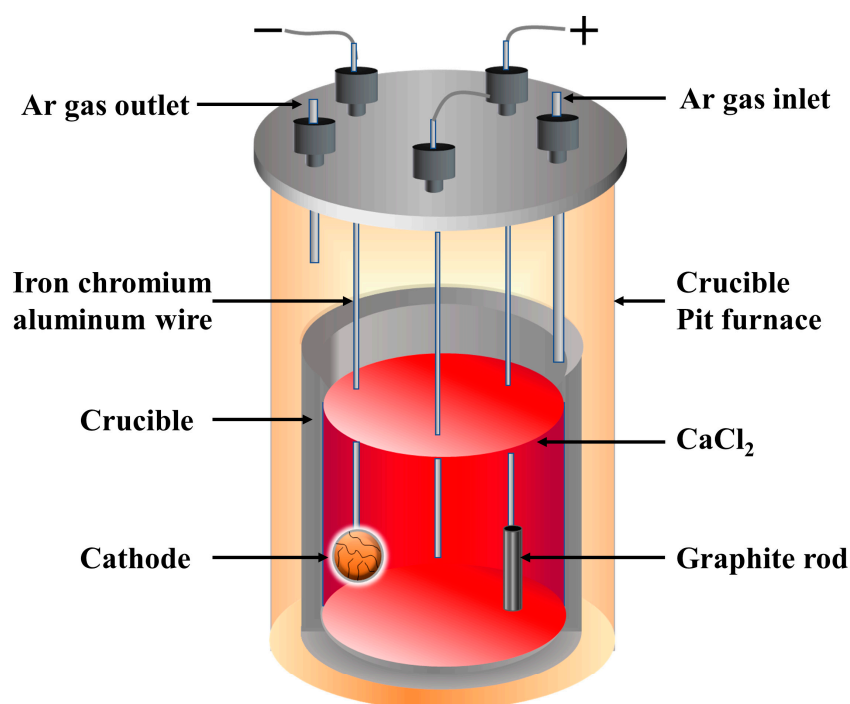


Figure 2. Schematic illustration of the experimental setup.

2.3. Experimental Principle

The Fe–Ti equilibrium phase diagram is shown in Figure 3. When $T > 882\text{ }^{\circ}\text{C}$, the crystal structure of titanium is a body-centered cubic β -titanium. In the temperature range from 595 to 1085 $^{\circ}\text{C}$, Ti:Fe $> 1:1$; FeTi and β -Ti (FeTi_4) can coexist in equilibrium.

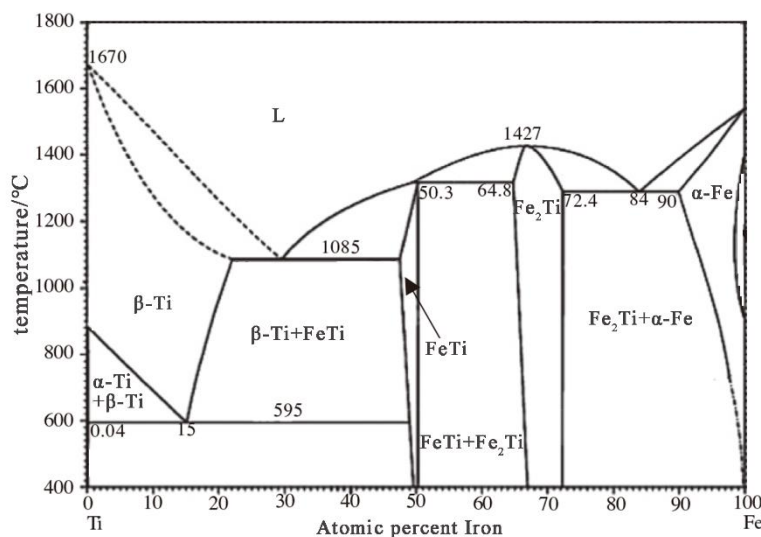


Figure 3. Fe–Ti equilibrium phase diagram.

Based on the principle of the FFC method, Ti–Fe alloys can be prepared through the molten salt electrochemical deoxidation process. The electrolytic voltage required for the electrochemical deoxidation process is 3.1 V, which is lower than the theoretical decomposition voltage of CaCl_2 (3.18 V) at 900 $^{\circ}\text{C}$ and higher than the theoretical decomposition voltage of TiO_2 and Fe_2O_3 . A schematic illustration of the reaction mechanism of the electrolysis process in this study is shown in Figure 4. According to the relevant literature reports [14–16], the intermediate products generated during the electrolysis of $\text{TiO}_2/\text{Fe}_2\text{O}_3$ mixtures commonly include Fe, CaTiO_3 , TiO_2 , TiO, and Fe_2Ti . The entire reduction process is complicated, and the valence state of titanium is gradually reduced during the electrochemical reduction process.

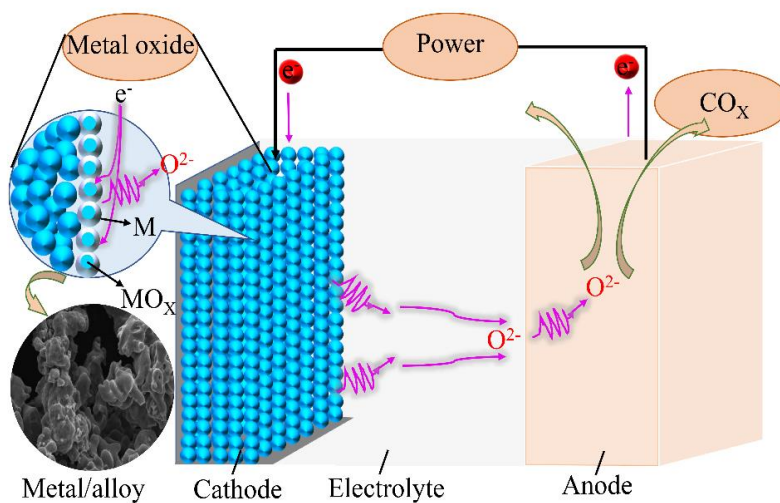


Figure 4. Schematic illustration of the reaction process during electrolysis.

In this study, initial theoretical analysis was performed using the thermodynamic database and thermodynamic software FactSage7.2. For a temperature range from 873 to 1273 K and a step change of

20 K, the ΔG^θ and the theoretical decomposition voltages (type 1) that describe the possible electrode reactions during the direct reduction process can be calculated. These calculations are given in Table 2. Origin software was used to linearly fit the calculated values to obtain the relationship between ΔG^θ and temperature, as shown in Figure 5.

Table 2. ΔG^θ and the theoretical decomposition voltage (E^θ) of the possible reactions that occurred during the electrolysis process.

Electrode Reaction	$\Delta G^\theta - T$	ΔG^θ (T = 1173 K)	E^θ
$2 \text{ TiO}_2 + 2 [\text{CaO}] = 2 \text{ CaTiO}_3 (\text{s})$	$-159.2 - 0.014T$ (1)	-175.622	-
$2 \text{ FeTiO}_3 (\text{s}) + 2 \text{ C} (\text{s}) = 2 \text{ Fe} (\text{s}) + 2 \text{ TiO}_2 (\text{s}) + 2 \text{ CO} (\text{g})$	$597.14 - 0.64T$ (2)	-153.58	-
$\text{Fe}_2\text{O}_3 + 3 \text{ C} = 2 \text{ Fe} + 3 \text{ CO}$	$472.40 - 0.510T$ (3)	-125.677	-
$2 \text{ CaTiO}_3 (\text{s}) + 2 \text{ C} (\text{s}) = 2 \text{ TiO} (\text{s}) + 2 [\text{CaO}] + 2 \text{ CO} (\text{g})$	$737.22 - 0.34T$ (4)	338.4	0.89
$\text{CaTiO}_3 (\text{s}) + 2 \text{ Fe} (\text{s}) + 2 \text{ C} (\text{s}) = \text{Fe}_2\text{Ti} (\text{s}) + [\text{CaO}] + 2 \text{ CO} (\text{g})$	$691.48 - 0.32T$ (5)	316.12	0.82
$2 \text{ TiO} (\text{s}) + 2 \text{ C} (\text{s}) = 2 \text{ Ti} (\text{s}) + 2 \text{ CO} (\text{g})$	$851.38 - 0.39T$ (6)	393.91	1.02
$4 \text{ TiO}_2 + 2 \text{ C} = 2 \text{ Ti}_2\text{O}_3 + 2 \text{ CO}$	$531.74 - 0.364T$ (7)	104.768	0.27
$2 \text{ Ti}_2\text{O}_3 + 2 \text{ C} = 4 \text{ TiO} + 2 \text{ CO}$	$622.89 - 0.326T$ (8)	240.492	0.62
$\text{CaTiO}_3 (\text{s}) + \text{Fe} (\text{s}) + 2 \text{ C} = \text{FeTi} (\text{s}) + [\text{CaO}] + 2 \text{ CO} (\text{g})$	$744.60 - 0.33T$ (9)	357.51	0.93
$2 \text{ TiO} (\text{s}) + 2 \text{ Fe} (\text{s}) + 2 \text{ C} (\text{s}) = 2 \text{ FeTi} (\text{s}) + 2 \text{ CO} (\text{g})$	$751.98 - 0.32T$ (10)	376.62	0.98
$2 \text{ TiO} (\text{s}) + 4 \text{ Fe} (\text{s}) + 2 \text{ C} (\text{s}) = 2 \text{ Fe}_2\text{Ti} (\text{s}) + 2 \text{ CO} (\text{g})$	$645.74 - 0.31T$ (11)	282.11	0.73

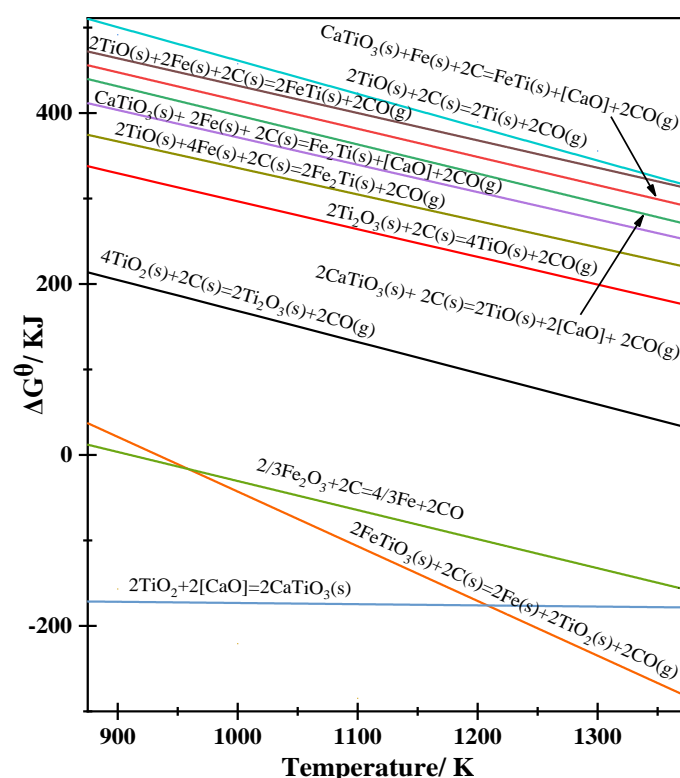


Figure 5. Relationship between ΔG^θ and the temperature of the possible reactions that occurred during the electrolysis process.

From the calculations presented in Table 2, we can determine the reactions that are likely to proceed during heating and the pre-electrolysis process based on the values of ΔG^θ in the given temperature range. For reaction 1, $\Delta G^\theta < 0$, which implies that CaTiO_3 can be generated as an intermediate product through the reaction. The presence of CaO in the sample results from impurities that exist in the form of Ca^{2+} and O^{2-} ions in the molten salt. When a potential is applied between the cathode and anode, reactions 1, 2, and 3 are likely to occur. Consequently, FeTiO_3 will decompose into Fe and CaTiO_3 , accompanied by the electrolysis of Fe_2O_3 to Fe (reaction 3). Simultaneously, the electrolytic reduction

of the intermediate products (CaTiO_3 and TiO_2 , as shown in reactions 4–9) will occur. The Fe generated will react with titanium to form Fe–Ti alloys, as shown in reactions 10 and 11, which include the FeTi and Fe_2Ti alloys. It should be noted that the alloy phases, such as FeTi and Fe_2Ti , will be affected by the content of the enriched Fe around CaTiO_3 [17].

During the electrolysis process, oxygen ions will migrate to the anode to produce CO or CO_2 . The electrode potentials of the impurity elements are listed in Table 3. In our previous research [18], we proved that impurities, such as the Ca, Al, and Si compounds, comprising the titanium-containing waste residue were reduced to their corresponding elements, and most of the impurities were removed as molten salts. Some of the remaining impurities were observed by washing the molten salt with hydrochloric acid. The corresponding chloride was dissolved in HCl washing solution, but some impurities may remain in the products after this process, owing to the blockage of the pores.

Table 3. Electrode potentials of impurity elements.

Elements	Electrode Reaction	Electrode Potential/V
Ca	$\text{Ca}^{2+} + 2\text{e}^- \rightarrow \text{Ca}$	−2.866
Si	$\text{Si}^{4+} + 4\text{e}^- \rightarrow \text{Si}$	−0.843
Al	$\text{Al}^{3+} + 3\text{e}^- \rightarrow \text{Al}$	−1.662

3. Results and Discussion

3.1. Mixed Oxide Cathode

The XRD patterns in Figure 6a,b illustrate the main phases present in the sample after high energy ball milling and high temperature heat treatment, respectively. Fe_2O_3 , TiO_2 , FeTi_2O_5 and Fe_2TiO_5 were identified in XRD patterns, and the particle size was reduced from 48.11 to 4.55 μm after milling, as listed in Table 4 and Figure 7.

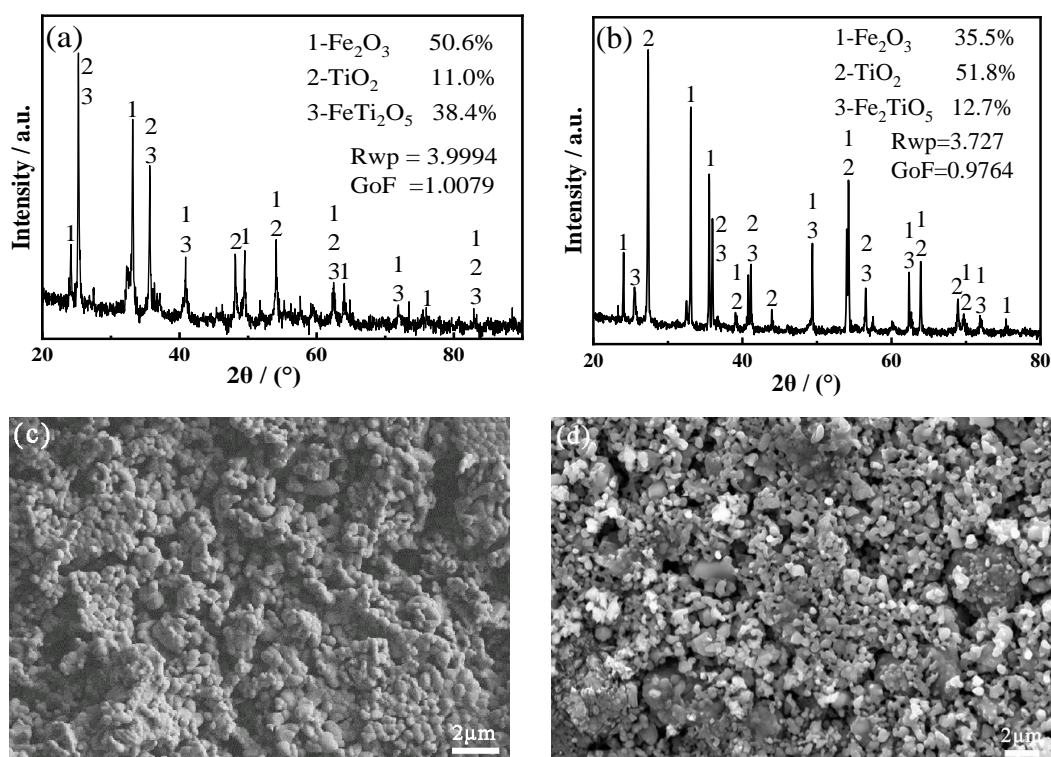
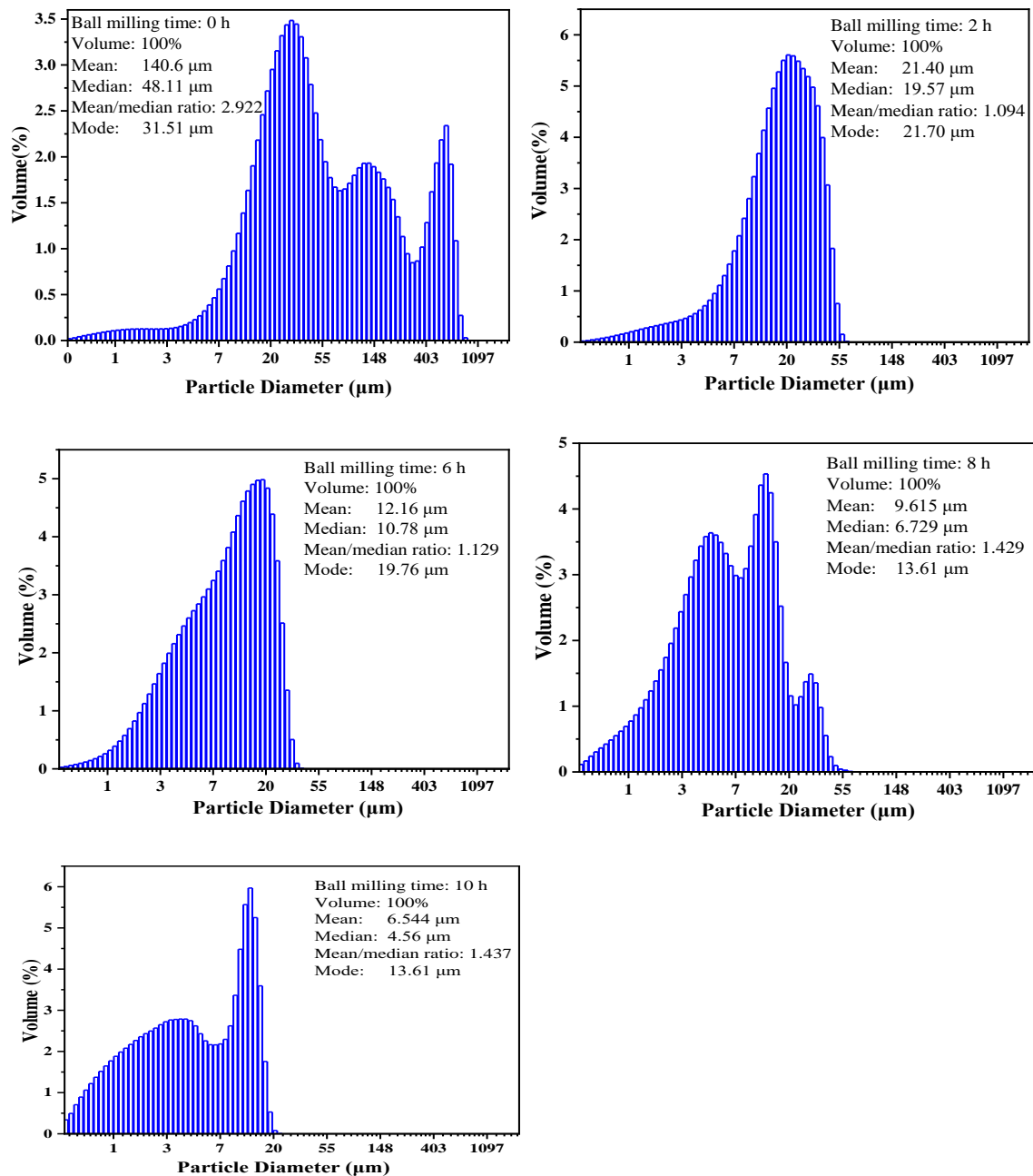


Figure 6. (a) XRD pattern before high energy ball milling; (b) XRD pattern after high energy ball milling; SEM images of the titanium-containing waste residue and Fe_2O_3 (c) before heat treatment and (d) after heat treatment.

Table 4. Particle size of the products after being milled for different durations.

Time	Raw Ore	2 h	6 h	8 h	10 h
Granularity (Median)	48.11 μm	19.57 μm	10.78 μm	6.73 μm	4.55 μm

**Figure 7.** Particle size distribution of the products after being milled for different durations.

The SEM images in Figure 6c,d illustrate the effect of the high-temperature heat treatment on the cathode material. After the sintering of the cathode material at high temperature, the porosity increased and the particles were interconnected with each other. The electrical conductivities of the sintered cathode pellets increased from 10^{-7} to 10^{-6} S/cm before sintering and up to 10^{-4} to 10^{-2} S/cm afterward.

3.2. Effect of Raw Material Ratio on the Morphology of the Product and Its Elemental Composition

The microstructures of the products obtained using different ratios of the raw material are shown in Figure 8a–e. As the proportion of Ti in the raw materials was increased, the particles of the product appeared more densely packed, which is consistent with the apparent increase in solubility from the macroscopic appearance in Figure 8f. Table 5 contains a summary of the elemental compositions of the products for which the atomic ratio of Ti and Fe in the product is similar. As the content of Ti in the electrolytic product increases, the quantity of the β -Ti(FeTi_4) phase increases, and the β -Ti phase takes the form of a metastable alloy $\text{Fe}_{1-x}\text{Ti}_x$ ($x < 0.8$) [19], which is a relatively dense alloy. This could be explained by the increased density of the cathode. At an atomic ratio of Ti:Fe = 1.2:1, the micromorphology of the product is more uniform and demonstrated a sponge-like structure.

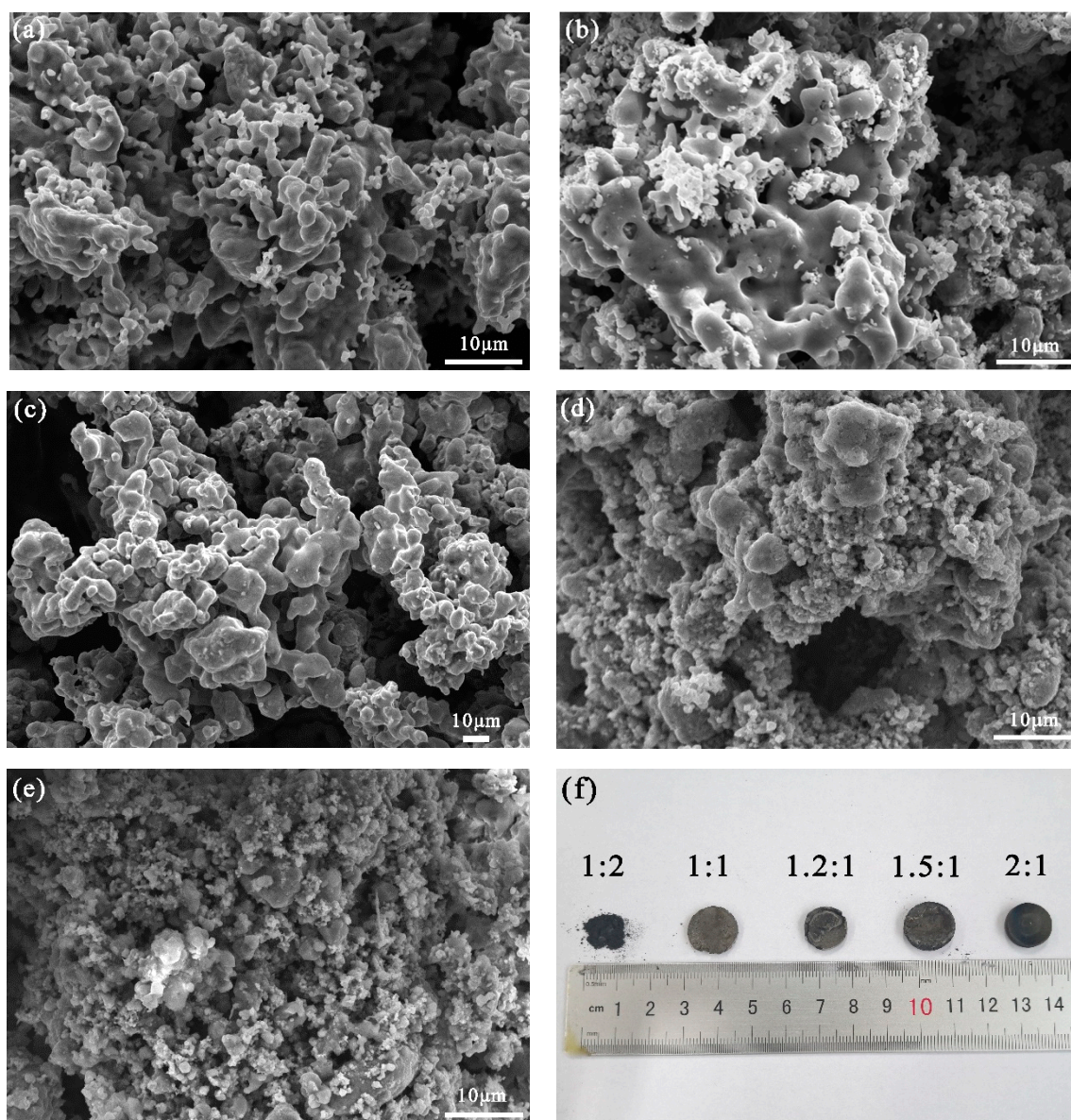


Figure 8. Microstructure of the product of the electrolysis of the raw materials with different Ti:Fe element ratios: (a) 1:2; (b) 1:1; (c) 1.2:1; (d) 1.5:1; (e) 2:1; (f) macroscopic appearances of the product of electrolysis corresponding to (a–e), respectively.

Table 5. Elemental contents (wt%) of the electrolytic products produced from raw materials with different Ti and Fe atomic ratios.

Ti:Fe	O	Ti	Fe	C	Si	Ca
1:2	1.95	24.53	65.3	7.65	0.57	-
1:1	2.08	45.63	45.82	5.04	1.43	-
1.2:1	0.69	49.34	45.43	2.67	1.87	-
1.5:1	2.05	44.62	47.69	2.02	2.1	1.52
2:1	6.49	57.4	29.92	2.06	2.04	2.09

The electrolytic product was analyzed by EDS for three times and the average values are shown in Table 5. With an increase in Ti, the C content in the product decreased, but impurities such as Si and Ca increased. A higher iron content, e.g., Ti:Fe = 1:2, will increase the electrical conductivity of the cathode and speed up the electrolytic process. Owing to the lower decomposition voltage of Fe, it was preferentially reduced compared to Ti, making the cathode material porous (Figure 8f). As the proportion of Fe atoms decreased, the content of FeTi₄ in the product increased, producing a dense cathode structure and limiting the infiltration of carbon powder; this explains the gradual decrease in the carbon content. Based on our previous research [20], the lower porosity limits the transfer of electrons and oxygen ions, and this affects the electrolysis process. This is also the primary reason for the gradual increase in impurities (O, Si, and Ca). The microstructure of the product is sensitive to the ratio of Ti:Fe. Based on these results, the optimum raw material composition for the production of Fe–Ti alloys is Ti:Fe = 1.2:1.

3.3. Effect of Raw Material Ratio on the Electrolysis Process

The XRD patterns of the products obtained from the raw materials with different elemental ratios are shown in Figure 9. FeTi, FeTi₄, TiO, and Fe₂Ti phases were identified in the XRD patterns. When the atomic ratio is Ti:Fe = 1:2, the primary phase of the product is Fe₂Ti. As the Fe atomic ratio decreased, the Fe₂Ti diffraction peak in the product gradually decreased. When Fe:Ti (atomic ratio) is ≤ 1, the primary phases in the products are FeTi and FeTi₄, and as the proportion of Ti atoms increased, the primary diffraction peak of FeTi₄ increased, and an intermediate product (TiO) was observed. Based on the thermodynamic relationship shown in Figure 5, Fe–Ti can be produced via two routes. One route is the direct formation of Fe₂Ti and FeTi through the reaction of CaTiO₃ with Fe in a single step, as expressed by reactions 5 and 9 in Table 2. The other route is the stepwise deoxidation of CaTiO₃ to produce TiO and Ti, which can further react with iron to form Fe–Ti alloys. According to a previous study [21], CaTiO₃ can be directly reduced to form Fe₂Ti or FeTi in the Fe-rich region. When the Fe content is low, Fe–Ti is primarily generated via the second route. The phases in the products produced from the raw materials with different ratios of Ti and Fe are summarized in Table 6, which is consistent with the observations in a previous study [22].

Table 6. Atomic ratio of Ti and Fe and the primary phase in the electrolytic products.

Atomic Ratio (Ti:Fe)	Ti	Fe	Main Phase	Rwp	GoF
1:2	27.11	61.50	Fe ₂ Ti: 73.2%; FeTi: 26.8	3.8886	0.9955
1:1	41.39	35.88	Fe ₂ Ti: 39.2%; FeTi: 58.8%; TiO: 2.0%	5.9063	1.1227
1.2:1	46.81	36.89	FeTi ₄ : 16.0%; FeTi: 84%	4.1006	1.0048
1.5:1	40.02	36.66	FeTi ₄ : 18.7%; FeTi: 44.3%; TiO: 37%	7.4289	1.1794
2:1	40.72	18.01	FeTi ₄ : 76.1%; FeTi: 12%; TiO: 11.9%	5.7525	1.0404

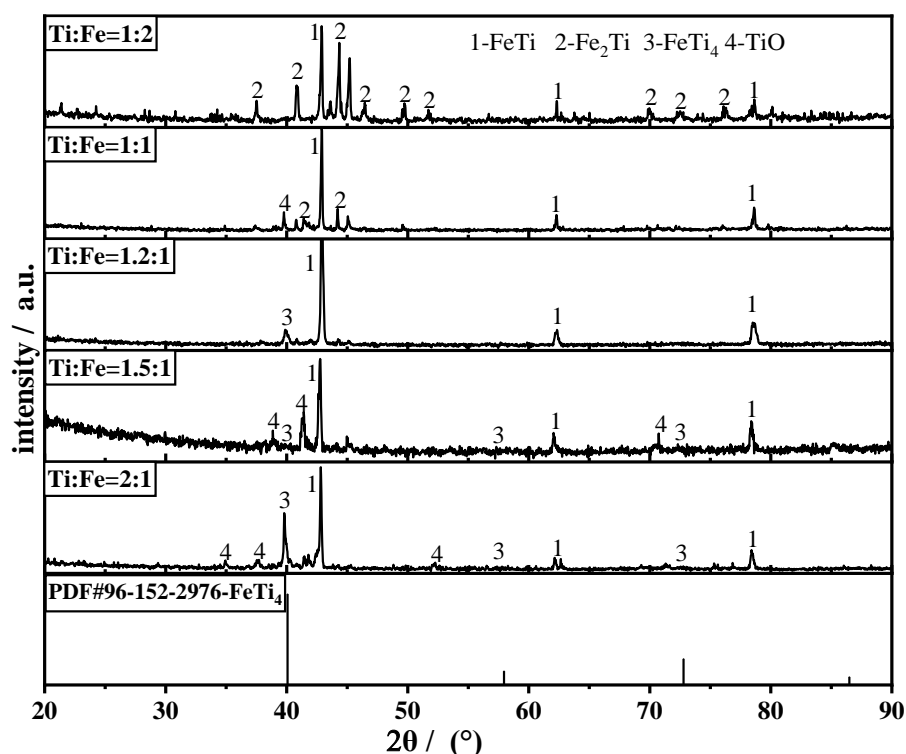


Figure 9. XRD patterns of the product obtained from the raw materials with different Ti and Fe atomic ratios.

3.4. Effect of the Duration of the Electrolysis Process on the Physical Properties of the Alloys

Considering the optimum composition of the raw materials with a Ti:Fe ratio of 1.2:1, the effects of the duration of the electrolysis process on the physical properties and electrochemical behavior of the alloys were investigated. The SEM images and XRD diffraction patterns of the products obtained after different durations of electrolysis are shown in Figure 10. In the early stage of electrolysis (0–1 h), owing to the deoxidation of Fe_2O_3 , the CaO content in the electrolyte increased rapidly (the maximum solubility of CaO in CaCl_2 molten salt is 19.4% [23]); this could promote reaction 1. The cathode comprised a large amount of CaTiO_3 produced from TiO_2 and CaO, resulting in particle fragmentation and blockage of the pores by the broken particles; this led to the formation of a dense cathode structure. During the electro-deoxidation process, O^{2-} was electrolyzed from the solid particles and diffused into the electrolyte through these pores; the electrolyte also penetrated these pores. Therefore, the porosity is also important for the deoxidation of CaTiO_3 . As the electrolysis progressed (1–3 h), TiO_2 was reduced to Ti or low-valence oxides; the intermediate product CaTiO_3 gradually transformed to Fe_2Ti and FeTi , which led to a decrease in the particle size and an increase in the bulk pores. This was primarily because of the formation of Fe–Ti alloy solid solution. Consequently, vacancies were formed in the bulk of the original CaTiO_3 particles, thereby increasing the porosity of the pellet. Finally, with the formation of FeTi and FeTi_4 , the structure of the product became dense and sponge-like. These observations are consistent with the results obtained from the thermodynamic analysis.

The electrochemical behavior of the cathode pellet in molten CaCl_2 at 900 °C was evaluated by cyclic voltammetry measurements at a scan rate of 20 mV/s. Three distinct reduction peaks at C_1 (−0.82 V), C_2 (0.26 V), and C_3 (1.6 V) were observed (Figure 11, curve A). The XRD analysis (Figure 9) demonstrated that the components of the cathode pellets after molten salt immersion are primarily CaTiO_3 , TiO_2 , and Fe_2O_3 . The peak potentials of C_1 and C_2 correspond to the theoretical decomposition voltages of reactions 5 ($E^\theta = 0.82$ V) and 7 ($E^\theta = 0.27$ V) respectively; hence, they could be attributed to the reduction of CaTiO_3 and TiO_2 to generate Fe_2Ti and Ti_2O_3 , respectively. This observation indicates that the two alloying routes occurred simultaneously. According to thermodynamic calculations,

the E^0 of the Fe_2O_3 reduction to produce Fe is negative, which indicates that this reaction proceeds spontaneously at a temperature of 1173 K. When a potential is applied, Fe_2O_3 ($E = -0.8486$ V) can be electrochemically reduced to Fe in a short time; therefore, no reduction peak was detected. Peak C_3 could be attributed to the cathodic formation of Ca in molten CaCl_2 [24,25]. As the electrolysis progressed, titanium oxides in the sample surface were reduced to Ti or low-valence oxides with a higher decomposition voltage; these oxides were easily oxidized, which caused a decrease in the oxidation peak potential. In this study, the potential of the A_1 peak decreased to -0.21 V (Figure 11, curve B).

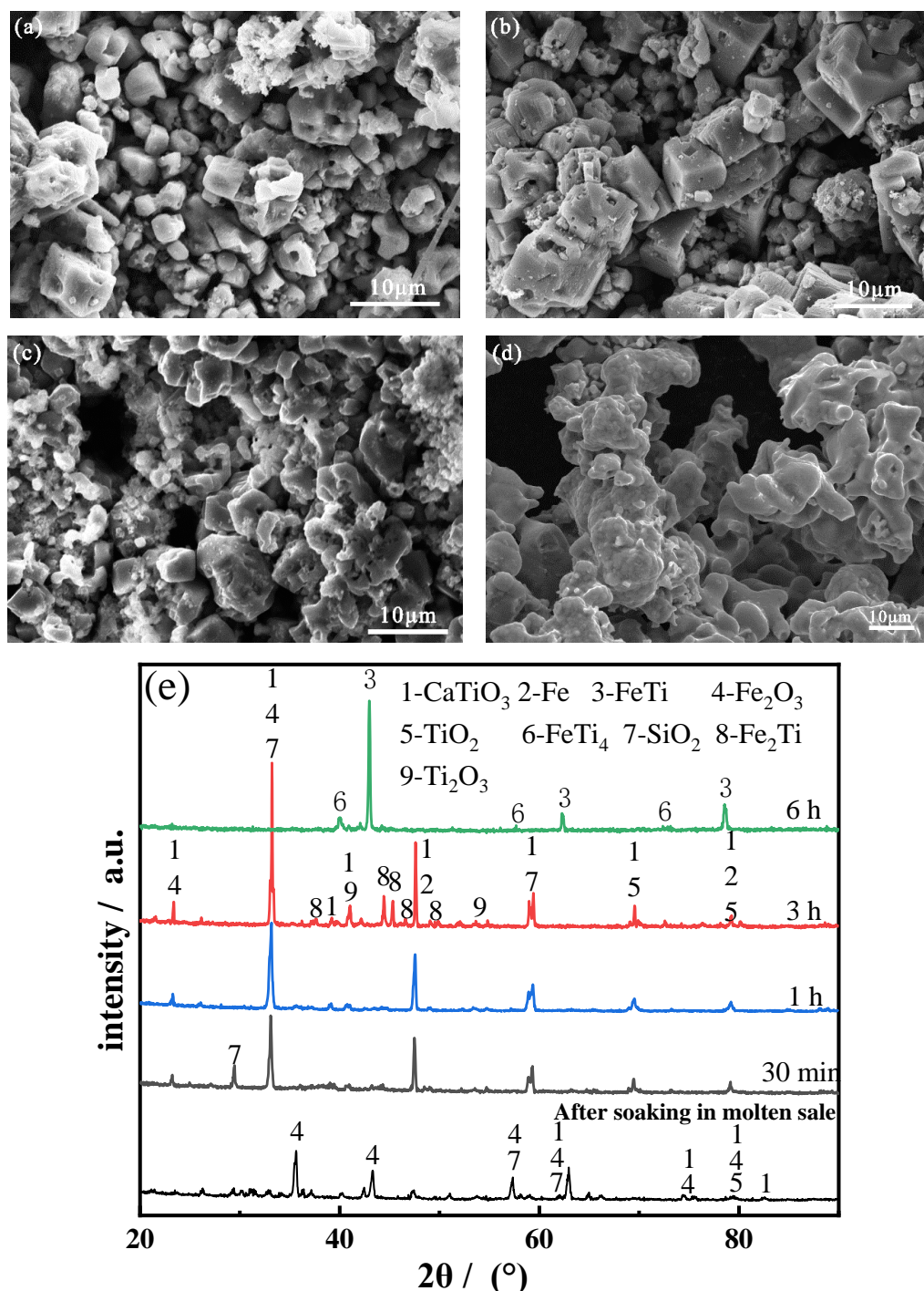


Figure 10. SEM images of the product electrolyzed for: (a) 30 min; (b) 1 h; (c) 3 h; (d) 6 h; (e) XRD diffractogram of the product electrolyzed for 30 min, 1, 3, and 6 h.

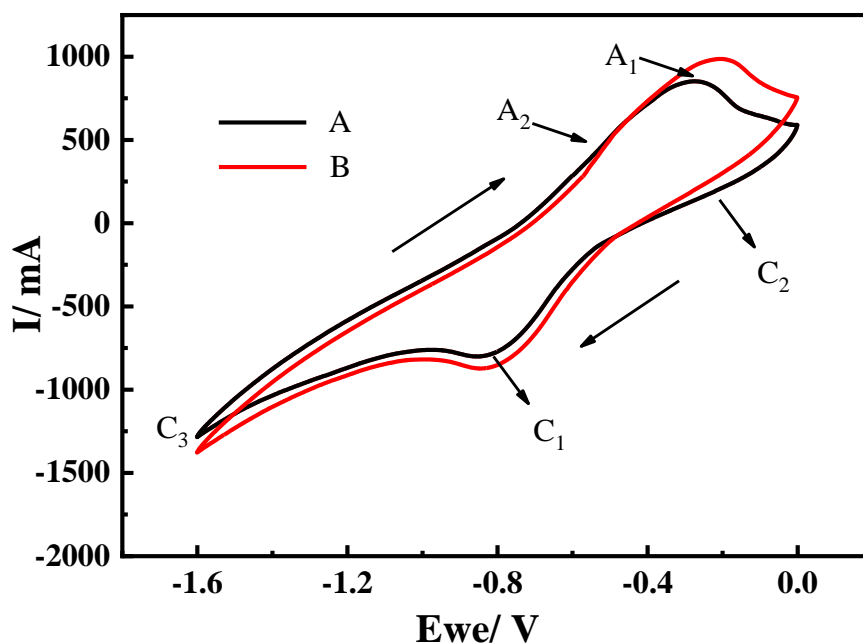


Figure 11. Cyclic voltammogram of the cathode pellet in molten CaCl_2 at: (A) $900\text{ }^\circ\text{C}$; (B) after testing for some time. Scan rate: 20 mVs^{-1} .

3.5. Effect of the Ratio of Raw Material on the Electrolysis Current

From the current–time curves recorded during the electrolysis process, as shown in Figure 12, there are three distinct stages. At the initial stage of electrolysis, the cathode was in close contact with nickel foam. Electroreduction reactions primarily occurred on the surface of the cathode pellet; therefore, the initial current was high (1.57 A). Within the next 100 min, a significant drop in current was observed, and oxygen on the surface of the cathode were gradually expelled. The O^{2-} diffusion distance increased, while the oxygen element in the low-valence titanium oxide was expelled from the lattice of the metal titanium. A high driving force was required to expel oxygen from the cathode, and this led to a decrease in the current [26]. In the case where a small amount of oxygen was to be ionized, the semiconductor cathode became conductive. The surface of the cathode became fully metalized when the current reached the lowest point.

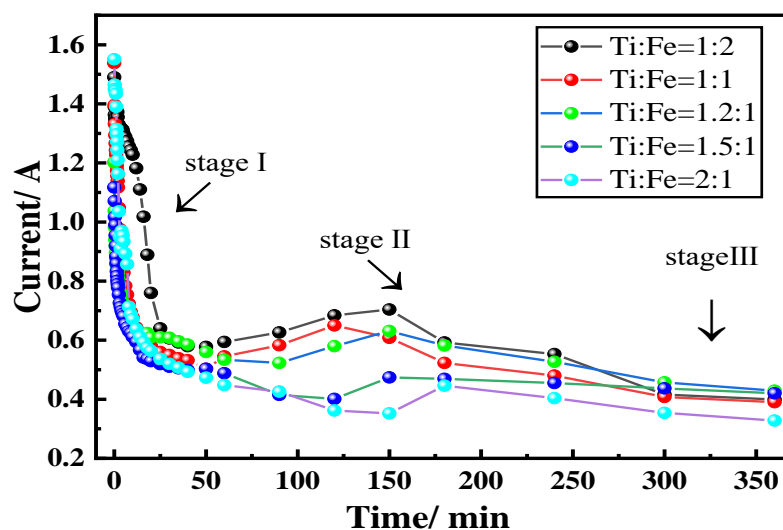


Figure 12. Current–time curves display the three stages of electrolysis of the raw materials with different Ti:Fe element ratios.

In the second stage, from 100 min to 5 h, the current increased, indicating that the electrolysis extended from the surface to the interior of the cathode, and the interior of the cathode was gradually metalized. The current plateaued when the electrolytic process was almost complete. Based on the results from a previous study [27], the current–time curve during electroreduction of metal oxide in molten CaCl_2 is dependent on the solubility of the oxygen in the metal. In the presence of dissolved oxygen, a peak was observed in the current profile; it gradually decreased to a stable current value, which was attributed to the background current.

Current efficiency is one of the technical indicators of an electrolytic process. The formula for calculating the current efficiency is as follows:

$$\eta = \frac{Q_{\text{theoretical}}}{Q_{\text{actual}}} * 100\% \quad (1)$$

$$Q_{\text{theoretical}} = \frac{Z \cdot F \cdot m_{\text{FeTi}}}{M_{\text{FeTi}}} \quad (2)$$

$$Q_{\text{actual}} = I * t \quad (3)$$

where η is the current efficiency; $Q_{\text{theoretical}}$ is the theoretically required quantity of electricity, the unit is C; and Q_{actual} is the actual electricity consumed, the unit is C. Z is the stoichiometric number of electrons required for the electrolysis reaction; F is Faraday constant, 96485 C/mol; m_{FeTi} is the mass of the actual product of FeTi, the unit is g; M_{FeTi} is the relative atomic mass of FeTi, 104 g/mol; I is the current used during the electrolytic process, the unit is A; and t is the duration of electrolysis, the unit is s. Table 7 lists the calculated values for current efficiency.

Table 7. Current efficiency of the electrolysis process with the raw material containing different Ti:Fe atomic ratios.

Atomic Ratio (Ti:Fe)	Current Efficiency
1:2	15.3243%
1:1	17.2082%
1.2:1	20.2135%
1.5:1	18.5583%
2:1	13.6615%

From the current–time curve and the stepwise reduction process of CaTiO_3 , a slow reduction rate of CaTiO_3 was observed, which became a limiting step during the entire electrolytic process. From the thermodynamic analysis, the reduction of CaTiO_3 was difficult. Simultaneously, because the crystal structure of CaTiO_3 is a body-centered cubic structure, this structure is stable, and more energy is required during the reduction process, thereby reducing the current efficiency.

4. Conclusions

The following conclusions were drawn from this study:

1. High-purity FeTi and FeTi₄ alloys were successfully prepared from the mixed titanium-containing waste slag and Fe₂O₃ by electrolysis at 900 °C and 3.1 V for 6 h in molten calcium chloride. As the atomic ratio of Ti increased, the Fe₂Ti phase decreased while that of FeTi₄ increased. The morphology of the product gradually became dense, and impurities such as carbon particles were absent in the dense structure of the FeTi and β -Ti alloys. A lower porosity of the pellet limited the transfer of electrons and oxygen ions, which would further limit the removal of oxygen ions and other impurity elements from the cathode pellet.
2. The alloying process of ferrotitanium can be divided into two routes, depending on the proportion of the iron atoms in the raw materials. When the atomic ratio of Ti and Fe is 1.2:1, both alloying

routes coexist simultaneously. At this atomic ratio, the microscopic morphology of the cathode is uniform and it displayed a sponge-like structure.

3. The current–time curve of the electrolytic process can be divided into three main stages. As the proportion of the iron atoms decreased, the time required for the start of the second stage and the current efficiency gradually decreased.

Author Contributions: Conceptualization, C.-y.C. and J.-q.L.; methodology, L.-z.W.; software, Y.-p.L.; validation, C.-y.C., J.-q.L. and Y.-p.L.; formal analysis, B.W.; investigation, S.-y.W.; resources, C.-y.C.; data curation, B.W.; writing—original draft preparation, B.W.; writing—review and editing, B.W.; visualization, B.W.; supervision, C.-y.C.; project administration, J.-q.L.; funding acquisition, C.-y.C. All authors have read and agreed to the published version of the manuscript.

Funding: This research was funded by “National Natural Science Foundation of China, grant number 51664005, 51774102, 52074096 and 51804088” and “Talent Team Giant [2017] 5626” and “Platform Talent KY (2015) 334” supported by the Talents of Guizhou Science and Technology Cooperation Platform.”

Conflicts of Interest: The authors declare no conflict of interest.

References

1. Kuenen, J. Ferro-Alloy Production. In *EMEP/EEA Emission Inventory Guidebook*; EEA: Copenhagen, Denmark, 2009; pp. 3–7.
2. Smirnov, L.A.; Grabeklis, A.A.; Demin, B.L. Processing slag from ferroalloy production. *Steel Transl.* **2009**, *39*, 93–96. [[CrossRef](#)]
3. Tripathy, P.K.; Gauthier, M.; Fray, D.J. Electrochemical Deoxidation of Titanium Foam in Molten Calcium Chloride. *Met. Mater. Trans. A* **2007**, *38*, 893–900. [[CrossRef](#)]
4. Zhao, K.; Wang, Y.; Gao, F. Electrochemical extraction of titanium from carbon-doped titanium dioxide precursors by electrolysis in chloride molten salt. *Ionics* **2019**, *25*, 6107–6114. [[CrossRef](#)]
5. Li, J.; Zhang, X.Y.; Liu, Y.B.; Li, Y.G.; Liu, R.P. Electrochemical behavior of tungsten in (NaCl-KCl-NaF-WO₃) molten salt. *Rare Met.* **2013**, *32*, 512. [[CrossRef](#)]
6. Chen, G.Z.; Fray, D.J.; Farthing, T.W. Direct Electrochemical Reduction of Titanium Dioxide to Titanium in Molten Calcium Chloride. *Nature* **2000**, *407*, 361–364. [[CrossRef](#)]
7. Han, W.; Li, M.; Zhang, M.-L.; Yan, Y.-D. Progress in preparation of rare earth metals and alloys by electrodeposition in molten salts. *Rare Met.* **2016**, *35*, 811–825. [[CrossRef](#)]
8. Zhou, Z.; Hua, Y.; Xu, C.; Li, J.; Li, Y.; Gong, K.; Ru, J.; Xiong, L. Preparation of Ferrotitanium from Ilmenite by Electrolysis-Assisted Calciothermic Reduction in CaCl₂-NaCl Molten Salt. *JOM* **2015**, *68*, 532–539. [[CrossRef](#)]
9. Tan, S.; Örs, T.; Aydınol, M.K.; Anikina, E.; Karakaya, I. Synthesis of FeTi from mixed oxide precursors. *J. Alloys Compd.* **2009**, *475*, 368–372. [[CrossRef](#)]
10. Panigrahi, M.; Iizuka, A.; Shibata, E.; Nakamura, T. Electrolytic reduction of mixed (Fe, Ti) oxide using molten calcium chloride electrolyte. *J. Alloys Compd.* **2013**, *550*, 545–552. [[CrossRef](#)]
11. Shi, R.M.; Bao, L.F.; Zhang, B. Effect of Temperature on the Ti-Fe Alloy Prepared by Molten Salt Electrolysis. *Adv. Mater. Res.* **2014**, *936*, 1189–1194. [[CrossRef](#)]
12. Du, J.; Li, Q.; Yang, S.; Yang, C.; Li, Z.; Xi, Z. Preparation of TiFe alloy by ilmenite electrolysis in molten salt. *Rare Met. Mater. Eng.* **2010**, *39*, 2247–2250.
13. Guo, X.; Guo, Z.; Wang, Z. Direct preparation of TiFe alloy by electrolytic reduction from TiO₂ and Fe₂O₃. *J. Univ. Sci. Technol. Beijing* **2008**, *30*, 620–624.
14. Ding, M.T. Ratio of magnesium in prepared high titanium ferroalloy with titanium concentrate and titanium slag by therite reduction. *Adv. Mater. Res.* **2012**, *581*, 1092–1095. [[CrossRef](#)]
15. Lu, X.; Zou, X.; Li, C.; Zhong, Q.; Ding, W.; Zhou, Z. Green Electrochemical Process Solid-Oxide Oxygen-Ion-Conducting Membrane (SOM): Direct Extraction of Ti-Fe Alloys from Natural Ilmenite. *Met. Mater. Trans. A* **2012**, *43*, 503–512. [[CrossRef](#)]
16. Mohanty, J. Electrolytic Reduction of Titania Slag in Molten Calcium Chloride Bath. *JOM* **2012**, *64*, 582–584. [[CrossRef](#)]
17. Li, Z.-Q.; Ru, L.-Y.; Bai, C.-G.; Zhang, N.; Wang, H.-H. Effect of sintering temperature on the electrolysis of TiO₂. *Int. J. Miner. Met. Mater.* **2012**, *19*, 636–641. [[CrossRef](#)]

18. Shen, Y.Y.; Chen, C.Y.; Li, J.Q. Preparation of titanium by SOM electrolytic process from ultrafine high titanium slag. *Rare Met. Mater. Eng.* **2019**, *48*, 1671–1676.
19. Panigrahi, M.; Shibata, E.; Iizuka, A.; Nakamura, T. Production of Fe-Ti alloy from mixed ilmenite and titanium dioxide by direct electrochemical reduction in molten calcium chloride. *Electrochim. Acta* **2013**, *93*, 143–151. [[CrossRef](#)]
20. Chen, C.; Yang, X.; Li, J.; Lu, X.; Yang, S. Direct Electrolytic Reduction of Solid Ta₂O₅ to Ta with SOM Process. *Met. Mater. Trans. A* **2016**, *47*, 1727–1735. [[CrossRef](#)]
21. Zhou, Z.; Hua, Y.; Xu, C.; Li, J.; Li, Y.; Zang, Q.; Zang, Y.; Kuang, W. Synthesis of micro-FeTi powders by direct electrochemical reduction of ilmenite in CaCl₂-NaCl molten salt. *Ionics* **2017**, *23*, 213–221. [[CrossRef](#)]
22. Wang, S.L.; Li, S.C.; Wan, L.F.; Wang, C.H. Electro-deoxidation of V₂O₃ in molten CaCl₂-NaCl-CaO. *Int. J. Miner. Met. Mater.* **2012**, *19*, 212. [[CrossRef](#)]
23. Wang, S.L.; Wang, W.; Li, S.C.; Cao, S.H. Cathodic behavior of molten CaCl₂-CaO and CaCl₂-NaCl-CaO. *Int. J. Miner. Met. Mater.* **2010**, *17*, 791. [[CrossRef](#)]
24. Rong, L.; He, R.; Wang, Z.; Peng, J.; Jin, X.; Chen, G.Z. Investigation of electrochemical reduction of GeO₂ to Ge in molten CaCl₂-NaCl. *Electrochim. Acta* **2014**, *147*, 352–359. [[CrossRef](#)]
25. Kartal, L.; Daryal, M.B.; Şireli, G.K.; Timur, S. One-step electrochemical reduction of stibnite concentrate in molten borax. *Int. J. Miner. Met. Mater.* **2019**, *26*, 1258–1265. [[CrossRef](#)]
26. Song, J.X.; Wang, Q.Y.; Hu, G.J.; Zhu, X.B.; Jiao, S.Q.; Zhu, H.M. Equilibrium between titanium ions and high-purity titanium electrorefining in a NaCl-KCl melt. *Int. J. Miner. Met. Mater.* **2014**, *21*, 660. [[CrossRef](#)]
27. Chen, S.; Liao, C.F.; Lin, J.Y.; Cai, B.Q.; Wang, X.; Jiao, Y.F. Electrical conductivity of molten LiF-DyF₃-Dy₂O₃-Cu₂O system for Dy-Cu intermediate alloy production. *Int. J. Miner. Met. Mater.* **2019**, *26*, 701–709. [[CrossRef](#)]

Publisher's Note: MDPI stays neutral with regard to jurisdictional claims in published maps and institutional affiliations.



© 2020 by the authors. Licensee MDPI, Basel, Switzerland. This article is an open access article distributed under the terms and conditions of the Creative Commons Attribution (CC BY) license (<http://creativecommons.org/licenses/by/4.0/>).